

Ramp and periodic dynamics across non-Ising critical points

Roopayan Ghosh, Arnab Sen, and K. Sengupta

Theoretical Physics Department, Indian Association for the Cultivation of Science, Kolkata-700032, India.

(Dated: January 16, 2018)

We study ramp and periodic dynamics of ultracold bosons in an one-dimensional (1D) optical lattice which supports quantum critical points separating a uniform and a Z_3 or Z_4 symmetry broken density-wave ground state. Our protocol involves both linear and periodic drives which takes the system from the uniform state to the quantum critical point (for linear drive protocol) or to the ordered state and back (for periodic drive protocols) via controlled variation of a parameter of the system Hamiltonian. We provide exact numerical computation, for finite-size boson chains with $L \leq 24$ using exact-diagonalization (ED), of the excitation density D , the wavefunction overlap F , and the excess energy Q at the end of the drive protocol. For the linear ramp protocol, we identify the range of ramp speeds for which D and Q shows Kibble-Zurek scaling. We find, based on numerical analysis with $L \leq 24$, that such scaling is consistent with that expected from critical exponents of the q -state Potts universality class with $q = 3, 4$. For periodic protocol, we show that the model display near-perfect dynamical freezing at specific frequencies; at these frequencies $D, Q \rightarrow 0$ and $|F| \rightarrow 1$. We provide a semi-analytic explanation of such freezing behavior and relate this phenomenon to a many-body version of Stuckelberg interference. We suggest experiments which can test our theory.

PACS numbers:

I. INTRODUCTION

The emulation of strongly interacting quantum model Hamiltonians using ultracold atom systems has seen tremendous experimental progress in recent years¹⁻⁴. Apart from allowing one to study phases and quantum phase transitions of well-known models, these experiments also provide unprecedented control over and tunability of the parameters of the model Hamiltonian they emulate. Therefore they serve as perfect test beds for studying quantum dynamics of several many-body systems. A study of such quantum dynamics often benefits from ultralow temperatures and isolation of the emulated systems from its environment. The present experiments satisfy these criteria and hence allow one to study dynamics of closed quantum systems^{1,4}.

One of the key achievements of the above-mentioned experiments in recent years have been realization of symmetry broken ground states of the emulated Hamiltonians^{2,3}. For example, states with broken Z_2 symmetry was realized sometimes back² using a tilted Bose-Hubbard model in its Mott state⁵. In this model, the tilt is generated by a spatially-varying Zeeman magnetic field which acts as an effective electric field for the neutral spin-one ($F = 1$) bosons. The Hamiltonian of such bosons in an one-dimensional optical lattice reads⁵

$$H_{\text{bosons}} = -J \sum_{\langle ij \rangle} (b_i^\dagger b_j + \text{h.c.}) - \sum_i (\mu + \mathcal{E}i) \hat{n}_i + U/2 \sum_i \hat{n}_i (\hat{n}_i - 1) \quad (1)$$

where U is the on-site interaction between the bosons, \mathcal{E} is the effective electric field, μ is the chemical potential, b_i denotes the boson annihilation operator at site i , $\hat{n}_i = b_i^\dagger b_i$, J denotes the nearest-neighbor boson hop-

ping amplitude, i the site coordinate and we have set the lattice spacing a to unity. It was shown in Ref. 5 that the Mott phase of this boson Hamiltonian can be well understood using an effective dipole model

$$H_d = -w \sum_\ell (d_\ell + d_\ell^\dagger) + (U - \mathcal{E}) \sum_i \hat{n}_\ell^d \quad (2)$$

where the dipole creation operator lives on a link ℓ between the sites i and j of the chain and can be written as $d_\ell = b_i b_j^\dagger / \sqrt{n_0(n_0 + 1)}$, n_0 is number of bosons per site in the parent Mott state, the dipole number operator is given by $\hat{n}_\ell^d = d_\ell^\dagger d_\ell$, and $w = \sqrt{n_0(n_0 + 1)}J$. The dipoles which constitute Eq. 2 obey two constraints: $\hat{n}_\ell^d \leq 1$ which corresponds to having at most one dipole on each link and $\hat{n}_{\ell+1}^d \hat{n}_\ell^d = 0$ which corresponds to absence of dipoles on adjacent links. The phases of this model constitutes a dipole vacuum (or uniform parent boson Mott state) and a Z_2 symmetry broken maximal dipole ground state which are separated by a quantum critical point belonging to Ising universality class at $U - \mathcal{E}_c \simeq -1.31 \sqrt{n_0(n_0 + 1)}$. Note that the constraint $n_{\ell+1}^d n_\ell^d = 0$ is key to realizing such a state. Such translational symmetry broken state was experimentally realized in Ref. 2. These dipole models have been generalized to higher dimensions⁶. The quantum dynamics of these models has also been studied in details⁷⁻¹².

It was noted in Ref. 13 that a simple extension of the Hamiltonian H_d may lead to generating translational symmetry broken ground states with broken Z_n symmetry with $n > 2$. This is achieved by adding an interaction term H_1 to H_d leading to

$$H_0 = H_d + H_1, \quad H_1 = \sum_{\ell_1 \ell_2} V_{\ell_1 \ell_2} \hat{n}_{\ell_1}^d \hat{n}_{\ell_2}^d \quad (3)$$

The presence of the interaction term controls the symmetry of the ground state in the regime where $\mathcal{E} \gg U$ where

dipole formation is favored. For $V_{\ell_1\ell_2} = 0$, the constraint $\hat{n}_\ell^d \hat{n}_{\ell+1}^d = 0$ leads to a Z_2 symmetry broken state as discussed above. In contrast, a choice of $V_{\ell\ell+2} = V_0 > 0$ (with $V_{\ell\ell+n} = 0$ for $n > 2$) leads to a state of one dipole for every three links and hence to a Z_3 symmetry broken state for large enough values of V_0 and \mathcal{E} . Similarly, a choice of $V_{\ell\ell+2}, V_{\ell\ell+3} = V_1 > 0$ leads to a Z_4 symmetry broken state for large enough V_1 and \mathcal{E} . Thus the Hamiltonian allows for a simple model for realization of ground states with broken Z_n symmetry. For $n = 3$ and $n = 4$, there exists a second order transition between the uniform and the translational symmetry broken ground states¹⁴. It was shown in Ref. 13, that for $n = 3$, the model has two integrable lines along $w^2 = (U - \mathcal{E})V_0 + V_0^2$; out of these the one with $V_0/w > 0$ hosts a quantum critical point belonging to the 3-state Potts universality class at $V_0/w = [(\sqrt{5} + 1)/2]^{5/2}$. For a further increase in V_0 , the universality class of this critical point is expected to change as one moves away from the integrable line; however, for systems with $L \leq 21$, finite-size scaling data appears to be consistent with exponents belonging to the 3-state Potts universality class indicating that such a change may only be reflected in larger system sizes^{13,15}. A similar situation occurs for the critical point separating the Z_4 symmetry broken and the uniform states. In contrast, the transitions to Z_n symmetry broken states with $n > 4$ are expected to be first-order from known results for two-dimensional classical q -state Potts models¹⁶. Thus emulation of this Hamiltonian in finite-size ultracold boson systems is expected to lead to experimental realization of quantum critical point belonging to Potts universality class; in what follows we shall study the ramp and periodic dynamics of this model with $V_0, V_1 \rightarrow \infty$.

More recently, such Z_3 and Z_4 symmetry broken states has been experimentally realized using a chain of Rydberg atoms with $L \leq 51$ sites³. The effective Hamiltonian describing such atoms can be written as

$$H_{\text{Ryd}} = \sum_i (\Omega \sigma_i^x + \Delta n_i) + \sum_{ij} V_{ij} n_i n_j \quad (4)$$

Here $n_i \leq 1$ denotes the number of (excited) Rydberg atoms on the i^{th} site of the chain, Δ denotes detuning parameter which can be used to excite an atom to a Rydberg state, V_{ij} denotes the interaction strength between two Rydberg atoms and can be varied by tuning the distance between them, and $\sigma_i^x = |r_i\rangle\langle g_i| + |g_i\rangle\langle r_i|$ denotes the coupling between the Rydberg ($|r_i\rangle$) and ground ($|g_i\rangle$) states. In the experiments, V_{ij} could be tuned so that, for example, $V_{i,i+1} \gg \Delta, \Omega$ and $V_{i,i+n} \ll \Delta, \Omega$ for $n > 1$ leading to realization of Z_2 symmetry broken ground state of Rydberg atoms for $\Delta \ll 0$. Other configurations of V_{ij} where $V_{i,i+n} \gg \Delta, \Omega$ for $n = 1, 2$ and $n = 1, 2, 3$ led to experimental realization of the Z_3 and Z_4 symmetry broken states respectively. These states are expected to be separated from the uniform Rydberg vacuum (where all the atoms are in the ground state) by quantum critical points with same universality class as that of H_0 (Eq. 3). A measurement of on-site num-

ber of Rydberg atoms confirmed the presence of these symmetry broken states. Moreover, Ref. 3 also studied the dynamics of this system following sudden quenches of the detuning parameter Δ across its critical value. It was shown that such quenches lead to oscillations of density-density correlations of the Rydberg atoms with unusually long decay times. However, the ramp and periodic dynamics of these systems with broken Z_3 and Z_4 symmetry states has not been studied either experimentally or theoretically.

In this work, we study both linear ramp and periodic dynamics of a boson system described by Eq. 3. We compute, using exact diagonalization (ED), the dipole number density n_d , the wavefunction overlap F , the excess energy Q , and the excitation density D of the bosons following either a ramp of the electric field \mathcal{E} from the dipole vacuum state to the quantum critical point or after a periodic drive across the quantum critical point. The main results that we obtain from such a study are as follows. First, for a linear ramp of electric field which takes the system from a dipole vacuum to the critical point, we identify the ramp rates for which D and Q obeys Kibble-Zurek scaling^{11,17,18}. Our analysis shows that such scalings, for systems with $L \leq 24$, are consistent with critical exponents of the two-dimensional classical 3-state and 4-state Potts models whose values are analytically known¹⁹; thus our results indicate the possibility of experimental verification of KZ scaling in a system with Potts critical exponents. Second, we compute n_d , F , D , and Q for a periodically varying electric field (characterized by a drive frequency ω_0), which takes the system through the critical point to the Z_3 or Z_4 symmetry broken phases and back, at the end of a single drive period ($t = T = 2\pi/\omega_0$). We show that all the above-mentioned quantities display non-monotonic behavior as a function of the drive frequency ω_0 ; in particular, we identify specific values of $\omega_0 = \omega_0^*$ for which $n_d(T)$, $D(T)$, $Q(T) \simeq 0$ and $|F| \simeq 1$ indicating near-perfect dynamic freezing^{20,21}. We analyze such dynamic freezing and show that it originates from a many-body generalized version of the Stueckelberg interference phenomenon²². Third, we study the amplitude of oscillations of dipole excitation density $D(t)$ for $t > T$ by allowing the system to evolve with $H(t=0)$ following a periodic drive for a single drive period. We find that the amplitude of such oscillations nearly vanish for $\omega_0 = \omega_0^*$; moreover, they scale linearly in $\delta\omega = |\omega_0 - \omega_0^*|$ around ω_0^* for any finite J . These observations provides an experimental route to verification of dynamic freezing phenomenon using similar measurements as those which have been already carried out in Ref. 3 for sudden quench protocol. Finally, we compare numerical results for periodic drive protocols obtained using dipole Hamiltonian (Eq. 2) and the Rydberg Hamiltonian (Eq. 4) and demonstrate that they provide qualitatively similar results for $L = 9$. This allows us to show that our numerical results carried out using the dipole Hamiltonian (Eq. 2) would be of direct relevance to the experimental system studied

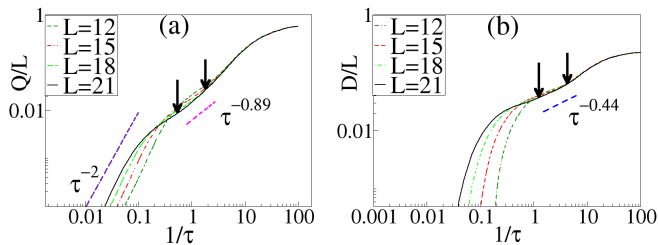


FIG. 1: (Color online) Linear ramp for boson systems for Z_3 symmetry broken state. In all of these plots the linear ramp takes the system from the uniform (symmetry unbroken) ground state to the critical point. The arrows indicate the extent of the Kibble-Zurek regime for the ramp rate τ^{-1} and dotted lines indicate the power-law scaling expected from theory. (a) Plot of Q/L as a function of the ramp rate τ^{-1} for several system sizes. (b) Plot of D/L as a function of the ramp rate τ^{-1} for several system sizes. All energies are scaled in units of U , L in units of the lattice spacing a , and τ in units of \hbar/U .

in Ref. 3.

The plan of the rest of the work is as follows. In Sec. II, we study the dynamics of the bosons under linear ramp protocol. This is followed by a study of the periodically driven boson systems in Sec. III. Finally, we discuss our main results, compare the dynamics of the dipole boson and the Rydberg Hamiltonian, suggest concrete experiments which can test our theory, and conclude in Sec. IV.

II. LINEAR RAMP

In this section we shall study a linear ramp protocol where the electric field \mathcal{E} in the dipole Hamiltonian given by Eq. 3 is varied linearly in time with a rate τ^{-1} :

$$\mathcal{E}(t) = \mathcal{E}_0 + (\mathcal{E}_f - \mathcal{E}_0)t/\tau \quad (5)$$

Here we choose \mathcal{E}_0 so that the ground state of the dipole Hamiltonian H_0 (Eq. 3) corresponds to dipole vacuum and \mathcal{E}_f denotes the final value of the electric field. In what follows, we shall ramp the electric field from \mathcal{E}_0 at $t = 0$ to \mathcal{E}_f at $t = \tau$ and measure D and Q at the end of this ramp. For the rest of this section we choose $\mathcal{E}_f = \mathcal{E}_c$ where \mathcal{E}_c denotes the critical value of the electric field. Numerically, we find, via exact diagonalization, $\mathcal{E}_c = U + 1.89[2.31]w$ for the critical points separating $Z_3[Z_4]$ ordered and the uniform state. We note that such a ramp is analogous to changing Δ in Eq. 4 linearly in time $\Delta(t) = \Delta_0 + (\Delta_f - \Delta_0)t/\tau$ with $\Delta_f = \Delta_c$ where the system is in Rydberg vacuum for $\Delta = \Delta_0$ and the critical point is at $\Delta = \Delta_c$. The similarity and difference between the dynamics of the two models shall be explored in details in Sec. IV.

To study the dynamics of the system, we first obtain the full set of eigenstates and eigenvalue of H_0 numerically

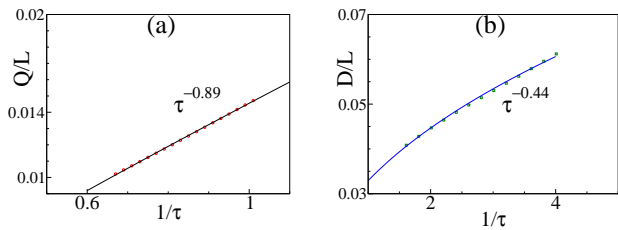


FIG. 2: (Color online) (a) Plot of Q/L as a function of $1/\tau$ for $L = 21$ in the Kibble-Zurek regime; the best fit corresponds to Kibble-Zurek exponent of 0.89 with a standard error of ± 0.005 . (b) D/L as a function of $1/\tau$ for $L = 21$ in the Kibble-Zurek regime; the best fit corresponds to the Kibble-Zurek exponent of 0.44 with a standard error of ± 0.005 . All other parameters are same as in Fig. 1.

ically using exact diagonalization for $\mathcal{E} = \mathcal{E}_f$ and for several system sizes ($L \leq 21(24)$ for $Z_3(Z_4)$ symmetry broken ground states). We denote the final (at $t = \tau$) eigenvalues and eigenstates as E_m^f and $|m\rangle_f$ respectively with $|1\rangle_f$ being the final ground state. In what follows, we shall use the final ground state energy as the reference for all energy measurement: $E_1^f = 0$. Further, in this section, we shall scale all energies in units of U , length in units of lattice spacing a , and time in units of \hbar/U .

Next, we note that the wavefunction, during any time $0 \leq t \leq \tau$, obeys the Schrodinger equation

$$\begin{aligned} i\hbar\partial_t|\psi(t)\rangle &= H_0(t)|\psi(t)\rangle = [H_0[\mathcal{E}_f] + \Delta H_0(t)]|\psi(t)\rangle \\ \Delta H_0(t) &= (\mathcal{E}_f - \mathcal{E}_0)(1 - t/\tau) \sum_{\ell} \hat{n}_{\ell}^d \end{aligned} \quad (6)$$

Since the wavefunction at any time t during the evolution, can be expressed in the $|m\rangle_f$ basis as

$$|\psi(t)\rangle = \sum_m c_m(t)|m\rangle_f. \quad (7)$$

Eq. 6 can then be written as a set of coupled equations for $c_m(t)$ which read

$$\begin{aligned} (i\hbar\partial_t - E_m^f)c_m(t) &= (\mathcal{E}_f - \mathcal{E}_0)(1 - t/\tau)\Lambda_{nm}(t) \\ \Lambda_{nm} &= \sum_n c_n(t) {}_f\langle m | \sum_{\ell} \hat{n}_{\ell}^d | n \rangle_f \end{aligned} \quad (8)$$

Here the matrix element Λ_{nm} is to be computed with respect to the eigenstates of the final Hamiltonian $H_0(t = \tau)$; thus the solution of the Schrodinger equation amounts to solving a set of coupled differential equations for $c_m(t)$. The initial condition for Eq. 8 is determined by $c_m(0) = \langle \psi_G | m \rangle$, where $|\psi_G\rangle$ denotes the initial ground state with $\mathcal{E} = \mathcal{E}_0$. Using the wavefunction obtained from this procedure, we can obtain expressions for several rel-

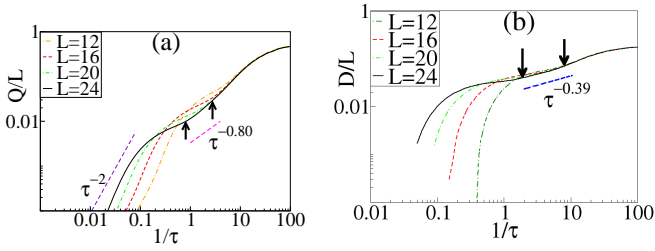


FIG. 3: (Color online) Same as in Fig. 1 but for boson systems with Z_4 symmetry broken state.

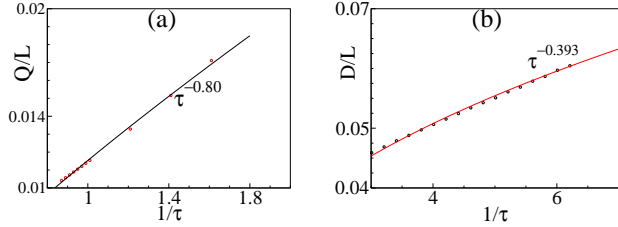


FIG. 4: (Color online) Same as in Fig. 2 but for boson systems with Z_4 symmetry broken state. The panels (a) and (b) show the best fit for Q/L and D/L with standard error of ± 0.005 and ± 0.01 respectively.

evant expectation values given by

$$\begin{aligned}
 n_d &= \frac{1}{L} \langle \psi(\tau) | \sum_l \hat{n}_l^d | \psi(\tau) \rangle = \frac{1}{L} \sum_{m,n} c_m^*(\tau) c_n(\tau) \Lambda_{mn} \\
 D &= n_d - \Lambda_{11}, \quad |F|^2 = |\langle 1 | \psi(\tau) \rangle|^2 = |c_1(t)|^2 \\
 Q &= \langle \psi(\tau) | H(\tau) | \psi(\tau) \rangle = \sum_{m \neq 1} E_m^f |c_m(\tau)|^2. \quad (9)
 \end{aligned}$$

It is well-known that in the thermodynamic limit, Q and F are expected to follow Kibble-Zurek scaling^{17,18} for arbitrarily slow drive: $Q \sim \tau^{-(d+z)\nu/(z\nu+1)}$ and $\ln F \sim \tau^{-d\nu/(z\nu+1)}$, where z and ν are the dynamical critical and correlation length exponents of the critical point. However, for finite-size system such scaling is seen only over a finite range of ramp rates^{10,23}. This can be simply understood by noting for that for very slow ramp, the system sees an effective system-size induced gap $\Delta_0 \sim 1/L$ at the critical point and thus displays a Landau-Zener behavior where excitation production is suppressed as $1/\tau^2$. It was shown in Ref. 23, that such a behavior is expected to set in for $\tau > \tau_c(L) \sim L^{1/\nu+z}$. Further for fast drives for which $\tau = \tau_{\text{fast}} \ll 1$, one expects the system wavefunction not have enough time to evolve during the drive leading to a plateau like feature for Q and F for all system sizes. In between for $\tau_c(L) \geq \tau \geq \tau_{\text{fast}}$, one expects the system to show universal scaling behavior. Such a scaling behavior may be expressed through

finite-size scaling functions^{10,23}

$$\begin{aligned}
 \ln F &\sim L^d \tau^{-d\nu/(z\nu+1)} s_1(L^{1/\nu+z}/\tau) \\
 Q &\sim L^d \tau^{-(d+z)\nu/(z\nu+1)} s_2(L^{1/\nu+z}/\tau) \quad (10)
 \end{aligned}$$

where the scaling functions $s_{1,2}$ satisfy $s_{1,2}(y \gg 1) \sim 1$, $s_1(y \ll 1) \sim y^{2-d\nu/(z\nu+1)}$, and $s_2(y \ll 1) \sim y^{2-(d+z)\nu/(z\nu+1)}$. We note that the precise values of $\tau_c(L)$ and τ_{fast} are non-universal numbers which depends on the symmetry and parameter values of the Hamiltonian and the system size; thus numerical determination of these help us to chart out the extent of the scaling regime for a given system size. Moreover, since for slow ramps D (which can be experimentally measured via parity of occupation measurements^{2,3}) represents deviation of the final state $|\psi(t)\rangle$ from the final ground state $|1\rangle$ and satisfies $D \ll 1$, we expect it to have analogous scaling as $\ln F$.

Next, we investigate the behavior of Q and D (Eq. 9) under the ramp protocol given by Eq. 5. The behavior of Q and D as a function of ramp rate τ^{-1} (measured in units of U/\hbar) and for several system sizes $L \leq 24$ is shown in Figs. 1 and 2 and Figs. 3 and 4 for the critical point separating the dipole vacuum and Z_3 and Z_4 symmetry broken states respectively. We find, that in accordance to the above-mentioned expectation, a finite region (marked by arrows in Figs. 1 and 3) where KZ scaling is evident; the width of this region increases with L . Below $\tau^{-1}\hbar/U \simeq 1$, the curves drops sharply with a slope of τ^{-2} reflecting the Landau-Zener behavior expected for finite system sizes. The numerical values of τ_c^{-1} and τ_{fast}^{-1} depends on the quantity measured; we find $\tau_c^{-1} \simeq 1$ for D and 0.7 for Q (see Figs. 2(a) and (b)) and $\tau_{\text{fast}}^{-1} \simeq 6$ (for D) and 2 (for Q) for the 3-state Potts critical point. Analogous numbers for the 4-state Potts critical point can be read from Figs. 4(a) and (b). Above τ_{fast}^{-1} , the behavior of Q and D deviates from the expected power-law signifying the setting in of fast drive regime. For $\tau^{-1}\hbar/U \geq 30$, we find different system sizes merge and show identical behavior indicating the setting in of the quench limit. We note that the expected value of the critical exponents $z = d = 1$ and $\nu = 5/6(2/3)$ for the 3(4)-state Potts critical point¹⁹ (here ν is not an integer unlike Ising universality); thus we expect $Q \sim \tau^{-10/11}$ and $D \sim \tau^{-5/11}$ for the 3-state and $Q \sim \tau^{-4/5}$ and $D \sim \tau^{-2/5}$ for the 4-state Potts critical points. Our data for D which shows a scaling of $\tau^{-0.44}$ (Figs. 1(b), and 2(b)) and $\tau^{-0.39}$ (Figs. 3(b) and 4(b)) show reasonably good match with expected theoretical results. A similar match occurs for Q for the 3 [4]-state Potts critical point for which we numerically find $\nu \simeq 0.9[0.8]$ as shown in Figs. 1(a) 2(a)[Figs. 3(a) and 4(a)].

We note that the scaling for Q in Figs. 1(a) and 3(a) predicts a slightly different range of τ for the Kibble-Zurek regime compared to that obtained from D ; this is a consequence of finite-size effect and is a reflection of non-universality of $\tau_c(L)$ and τ_{fast} . Moreover, we have checked that $\ln F$ do not display a significant Kibble-Zurek regime

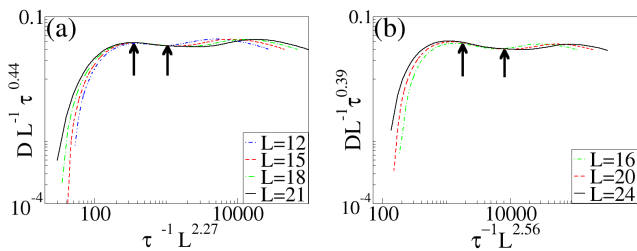


FIG. 5: (Color online) Linear ramp for boson systems for Z_3 (panels (a) and (b)) and Z_4 (panels (c) and (d)) symmetry broken states. In all of these plots the linear ramp takes the system from the uniform (symmetry unbroken) ground state to the critical point. The powers of L and τ in the plots are obtained using Eq. 10 with $z = d = 1$ and by choosing ν which yields best fit for numerical data. The arrows indicate the position of the Kibble-Zurek regimes as obtained in Figs. 1 and 3. All quantities are scaled with same units as mentioned in Fig. 1. See text for details.

for the range of system sizes studied here; this is analogous to its behavior obtained in Ref. 10 where it was also found to display Kibble-Zurek scaling for larger system sizes than studied here. Accessing such large system sizes is outside the scope of the exact diagonalization based study we carry out here.

Finally, we test our numerical data for D against the finite size scaling results (Eq. 10) for $1 \leq \tau^{-1} \leq 5$ where Kibble-Zurek scaling is expected to hold. The result from such a comparison is shown in Fig. 5. We note that Eq. 10 predicts that a plot of $\ln FL^{-d} \tau^{d+z} \nu / (z\nu+1)$, or equivalently $DL^{-d} \tau^{d+z} \nu / (z\nu+1)$, as a function of $L^{1/\nu+z} \tau^{-1}$ should be independent of L in the scaling regime. In Fig. 5(a), we plot $DL^{-d} \tau^{d+z} \nu / (z\nu+1)$ as a function of $L^{1/\nu+z} \tau^{-1}$ for the 3-state Potts critical point to test this prediction by choosing $z = d = 1$ and by varying ν to obtain the best fit to the scaling prediction. A similar plot for 4-state Potts critical point is shown in Fig. 5(b). We find that the optimal value of the correlation length exponent obtained from both the plots correspond to $\nu = 0.79 \pm 0.05 [0.64 \pm 0.03]$ for the 3[4]-state Potts critical point which shows reasonable match to both the numerical results obtained from Figs. 1.4 and theoretical values¹⁹. Moreover, the Kibble-Zurek regime obtained from these plots (shown by arrows in Fig. 5) coincide with those obtained from Figs. 1 and 3. Our analysis thus shows that even with system sizes $L \sim 20$, it is possible to find Kibble-Zurek scaling exponents for excitation production in these systems²⁴; moreover, the range of ramp rates over which such scaling is expected to be seen can be identified using our analysis. Importantly, we find that such scaling behavior manifest themselves in D which can be measured in standard experiments in ultracold atom systems; we shall discuss this in details in Sec. IV.

III. PERIODIC DRIVE

In this section, we consider the periodic dynamics of H_0 by varying the electric field periodically as a function of time according to the protocol

$$\mathcal{E}(t) = \mathcal{E}_0 - \mathcal{E}_1 \cos(\omega_0 t) \quad (11)$$

In what follows we shall choose $\mathcal{E}_0 = U$ and $\mathcal{E}_1 > 0 \gg w$, so that the system resides in the dipole vacuum state at $t = 0$. With this choice of protocol, the system crosses the critical point at $t_1 = t_0$ and $t_2 = T - t_0$ where $t_0 = \arccos[(U - \mathcal{E}_c)/\mathcal{E}_1]/\omega_0 \simeq \pi/(2\omega_0)$ and $T = 2\pi/\omega_0$ is the time period. In what follows, we shall scale all energies in units of $(U - \mathcal{E}(t = 0)) = \mathcal{E}_1$.

With the protocol given by Eq. 11, we study two aspects of the dynamics. The first involves measurement of n_d , D , Q , and F after a single drive protocol where the measured quantities are evaluated immediately after a drive cycle at $t = T$. This is done by computing expectation value of the relevant operators with respect $|\psi(t = T)\rangle$. The second, which mimics the experimental procedure carried out in Ref. 3, involves driving the system with $\mathcal{E} = \mathcal{E}(t)$ (Eq. 11) till $t = T$ followed by tracking its evolution with $H_0(t = 0) = H_0(t = T)$ for $t > T$ when the drive is switched off. For the second protocol, we shall track the behavior of the excitation density D as a function of time for $t > T$. Note that the knowledge $|\psi(T)\rangle$ is essential in tracking such evolution since it provides the initial value of $|\psi(t)\rangle$ during its evolution for $t > T$. The evolution of $D(t)$ for $t > T$ can be written as

$$D(t) = \sum_{m,n} \left(c_m^* c_n e^{i(E_n^f - E_m^f)(t-T)/\hbar} \Lambda_{mn} + \text{h.c.} \right) - \Lambda_{11} \\ c_m = f \langle m | \psi(T) \rangle. \quad (12)$$

In what follows, we are going to concentrate on the time average amplitude of these oscillations

$$D^{\text{av}} = \langle D(t) \rangle_{T_0} = \frac{1}{T_0} \int_0^{T_0} D(t) \quad (13)$$

where $\omega_0 T_0 \gg 1$ and we have chosen that a small change in T_0 do not lead to significant change in D^{av} .

The key features that we notice in the first aspect of the dynamics of the driven Hamiltonian is that n_d , D , Q , and F show non-monotonic behavior as a function of ω_0 . This is shown in Fig. 6 where we study the behavior of these quantities as a function of time during a single drive cycle. We find that there are special drive frequencies $\omega_0 = \omega_0^*$, which corresponds to the position of the minima in Fig. 6, for which the system, after a full period of the drive, comes remarkably close to the starting ground state exhibiting near-perfect dynamic freezing^{20,21}. Consequently, $Q, D \rightarrow 0$ and $F \rightarrow 1$ at $t = T$ for these frequencies; moreover in our case since we choose the starting state to be the dipole vacuum, one also has $n_d \rightarrow 0$ at these freezing frequencies. We note that this phenomenon is independent of both the symmetry of the

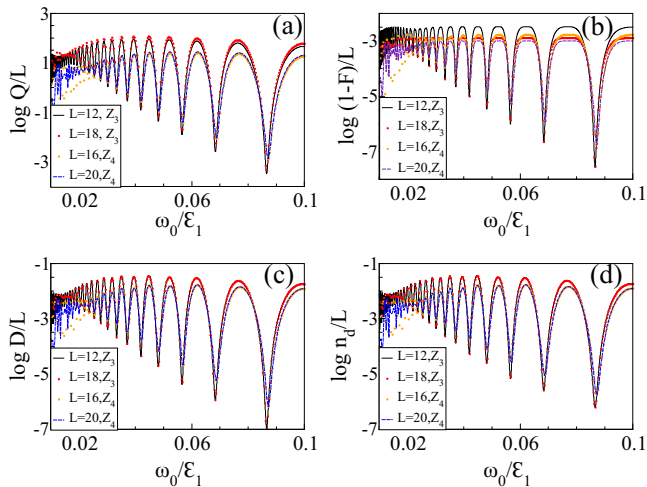


FIG. 6: (Color online) Periodic drive for boson systems for Z_3 and Z_4 symmetry broken states for several system sizes. In all of these plots the drive takes the system from the uniform (symmetry unbroken) ground state to the symmetry broken phase through the critical point and back. All data are shown for $t = T$. (a) Plot of $\log Q/L$ as a function of the drive frequency ω_0 showing distinct dips in values of Q at specific frequencies. (b) (c) and (d) Similar plots for Plot of $\log(1 - F)/L$, $\log D/L$, and $\log n_d/L$ respectively as a function of ω_0 , showing identical behavior. Here L is scaled in units of lattice spacing a and Q in units of \mathcal{E}_1 . See text for details.

critical point and the system size as can be clearly seen from Fig. 6. Furthermore, it is also different from the standard high-frequency freezing which originates from the inability of a quantum system to follow too fast a drive; this can be seen from the non-monotonicity Q , F , D and n_d as a function of the drive frequency.

The above-mentioned freezing phenomenon may be understood from the plot of wavefunction overlap amplitudes $|c_\alpha|^2 = |\langle \alpha | \psi(t) \rangle|^2$ of various eigenstates $|\alpha\rangle$ of the final Hamiltonian with the state $|\psi(t)\rangle$ as shown in Fig. 7. This is done in Fig. 7(a)[(b)] for $\omega_0/\mathcal{E}_1 = 0.0866[0.0776]$ where $D(T)$ shows a minimum [maximum]. We find that in both case, the wavefunctions starts in the ground state of H_0 which corresponds to the dipole vacuum state $|\alpha = 1\rangle \equiv |1\rangle$. Till the first crossing of the critical point which occurs at $t = t_0 \simeq \pi/(2\omega_0)$, the maximal weight of the system wavefunction stays at $|1\rangle$. At the first crossing, the $|1\rangle$ state hybridizes with several other states with finite dipole densities; thus the wavefunction after the first crossing stays in a linear superposition of several eigenstates and can be written as

$$|\psi(t_0 \leq t \leq T - t_0)\rangle \simeq \sum_{\alpha=1,16,91,231} c_\alpha(t) |\alpha\rangle \quad (14)$$

This behavior turns out to be similar for both values of the drive frequencies. However, the crucial difference between the two drive frequencies can be noted after the second passage through the critical point at

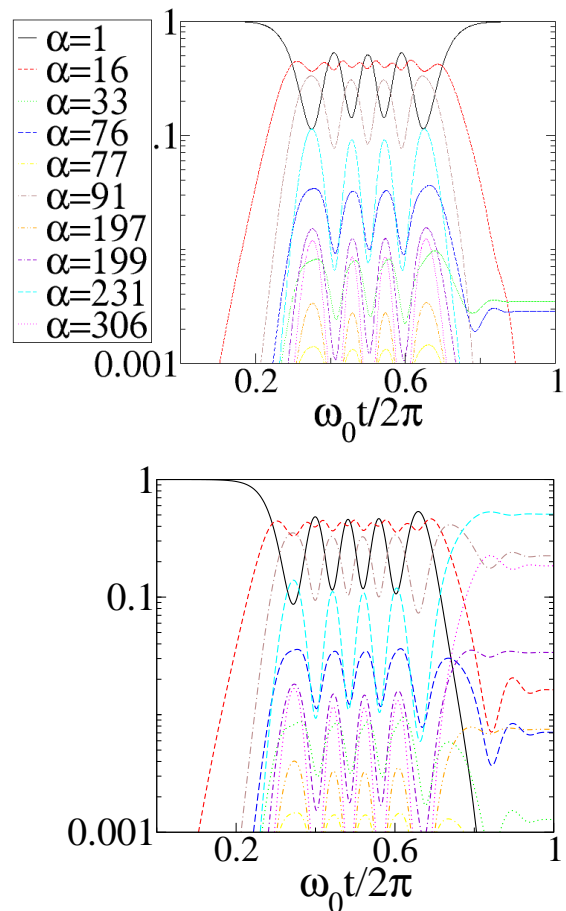


FIG. 7: (Color online) A plot of the wavefunction overlap amplitudes $|c_\alpha(T)|^2$ for all α for which $|c_\alpha(T)|^2 \geq 10^{-3}$. (a) Plot for $\omega_0/\mathcal{E}_1 = 0.0866$ which corresponds to a minima of $D(T)$ (b) Plot for $\omega_1/\mathcal{E}_1 = 0.0776$ for which $D(T)$ turns out to be a maximum. The crossings at the critical point occurs at $t = t_{1c}$ and t_{2c} where $\omega_0 t_{1(2)c}/(2\pi) = 0.25(0.75)$. See text for details.

$t = T - t_0 \simeq 3\pi/(2\omega_0)$. As shown in Fig. 7(a), for $\omega_1/\mathcal{E}_1 = 0.0866$, for $T \geq t > T - t_0$, the interference between these eigenstates (Eq. 14) ensures that $|c_1|^2 \rightarrow 1$ at $t > T - t_0$ while $|c_{\alpha \neq 1}|^2 \rightarrow 0$. This leads to a near-perfect overlap with the initial ground state. In contrast, at other drive frequencies, as shown in Fig. 7(b), $|c_1|^2 \rightarrow 0$ and the system tend to reside in a linear superposition of a number of states. For example, for $\omega_0/\mathcal{E}_1 = 0.0776$ chosen here, the system wavefunction resides in a superposition of states $|16\rangle$, $|91\rangle$, and $|231\rangle$ for $t > T - t_0$. This difference originates from the quantum interference between several eigenstates (Eq. 14) at the second crossing through the critical point and thus constitutes a many-body generalization of the Stueckelberg interference phenomenon²². At frequencies ω_0^* , where near-perfect dynamic freezing occurs, such quantum interference almost completely prohibits excitation production leading to near-perfect dynamic freezing.

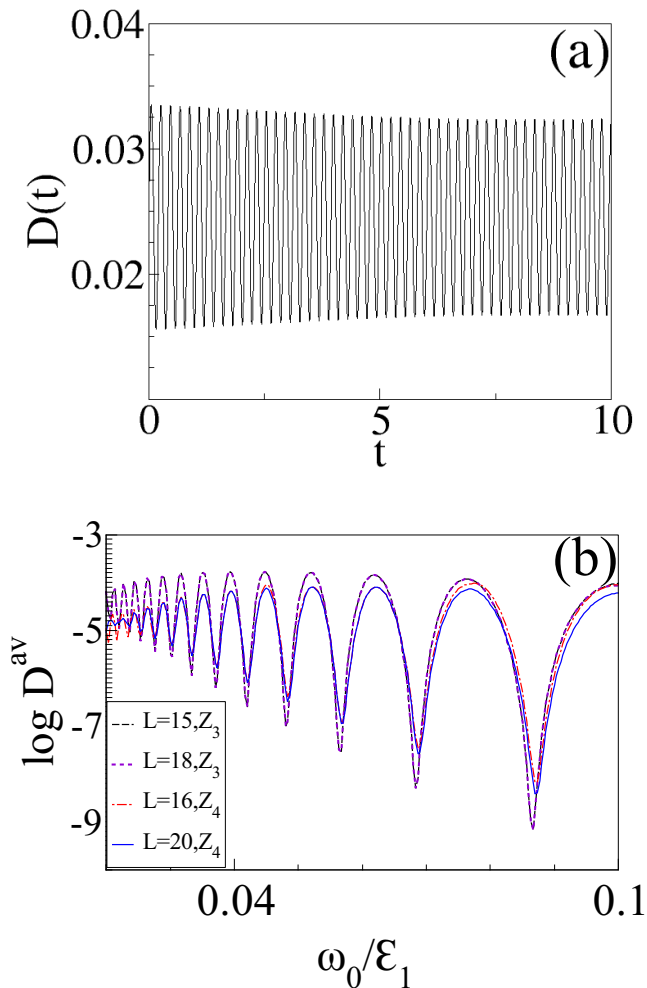


FIG. 8: (Color online) (a) Transient oscillations as a function of time t (in units of \hbar/w) after a complete cycle of drive for $D(t)$ for $\omega_0/\mathcal{E}_1 = 0.07$. (b) Plot of $\ln D^{\text{av}}$ with $T_0 = 10T$ as a function of ω_0 showing clear dips in the amplitude oscillations at specific frequencies where near-perfect dynamic freezing occurs. Here L is scaled in units of lattice spacing a . See text for details.

Finally, we address the average amplitude of oscillation of $D(t)$ for $t > T$ following a periodic ramp with frequency ω_0 from $t = 0$ till $t = T$. These oscillations are plotted as a function of time in Fig. 8(a). We find that the oscillations of $D(t)$ are quite robust and persists for $t \gg T$. The average amplitude D^{av} for $T_0 = 10T$ is shown in Fig. 8(b). We note from Eqs. 12 and 13 that $D^{\text{av}} \simeq \sum_m |c_m(t)|^2 \Lambda_{mm} - \Lambda_{11}$ for large T_0 since in this limit only the diagonal terms in Eq. 12 is expected to contribute to the amplitude. We find that the amplitude oscillations depends on both the wavefunction overlaps c_m and the matrix element Λ_{mm} . Thus it is expected to be large when the system wavefunction after the drive at $t = T$ is spread over several eigenstates of H_0 with non-zero $\langle \hat{n}_d \rangle$. In contrast, the amplitude is expected to

be near zero if the final wavefunction is very close to the final ground state. Thus the frequency dependence of D^{av} shows distinct minima at $\omega_0 = \omega_0^*$; this allows one to infer the freezing frequencies from the average oscillation amplitude of D^{av} . We shall discuss the experimental implication of this result in Sec. IV.

We note that near the freezing point at $\omega_0^*/\mathcal{E}_1 = 0.0866$, the wavefunction of the system can be described by $|\psi(T)\rangle \simeq c_1(T)|1\rangle + c_{16}(T)|16\rangle$ since $|c_m(T)|^2 \rightarrow 0$ for all $m \neq 1, 16$. The state $|16\rangle$ corresponds to a linear superposition of single dipole states which is also the first excited state of the system for $U - \mathcal{E} \gg 0$. Further numerically we find that for $\delta\omega = \omega_0 - \omega_0^*$ which satisfies $|\delta\omega| \ll \omega_0^*$, $|c_1(t)|^2 \sim 1 - (\delta\omega/\omega_0^*)^2$ and $|c_{16}(t)|^2 \sim (\delta\omega/\omega_0^*)^2$. Moreover, due to presence of a finite J term in the effective dipole Hamiltonian (Eq. 3), dipole number is not conserved. This allows for a finite matrix element of the dipole density operator \hat{n}_d between $|1\rangle$ and $|16\rangle$: $\langle 0|\hat{n}_d|16\rangle \sim J \neq 0$. Thus one can write

$$D(T; \omega_0 = \omega_0^* + \delta\omega) \simeq 2\text{Re}(c_0^* c_{16}) \langle 0|\hat{n}_d|16\rangle \sim \delta\omega, \quad (15)$$

where we have neglected higher order contributions, in $\delta\omega/\omega_0^*$, to $D(T)$. This explains the linear behavior of $D(T)$ and hence D^{av} around the crossing points. We note that the matrix element $\langle 0|\hat{n}_d|16\rangle$ would vanish in the Mott limit where $J = 0$ and we expect the variation of $D(T)$ around the crossing point to be quadratic in $\delta\omega$ in that limit.

IV. DISCUSSION

In this work we have studied the ramp and periodic dynamics of a Bose-Hubbard model in its Mott state in the presence of an electric field which supports Z_3 and Z_4 translational symmetry broken bosonic ground states. These states are separated from the uniform Mott state by 3- and 4- state Potts critical point. Our studies focuses on the property of such boson systems in the presence of a ramp or periodic drive which takes it out of equilibrium.

For the linear ramp protocol, we focus on a linear ramp with fixed rate τ^{-1} which takes the bosons system from its translational invariant ground state to the critical point. We show that the excitation density D and the residual energy Q exhibits Kibble-Zurek scaling. However, owing to the finite sizes of the boson chains that we have numerically analyzed, such scaling shows up over a finite range of ramp rates. We chart out these ramp rates, analyze our numerical data using a finite-size scaling ansatz, and obtain the critical exponent ν from such an analysis. The numerical values of the exponent ν that we obtain match quite well with the theoretical values for the 3- and 4-state Potts model for these system sizes. We note that such Z_3 and Z_4 translation symmetry broken states have been recently generated in finite size Rydberg chains³; it would be interesting to see if such chains also host a critical point in the same universality class. We note that our analysis could be of relevance

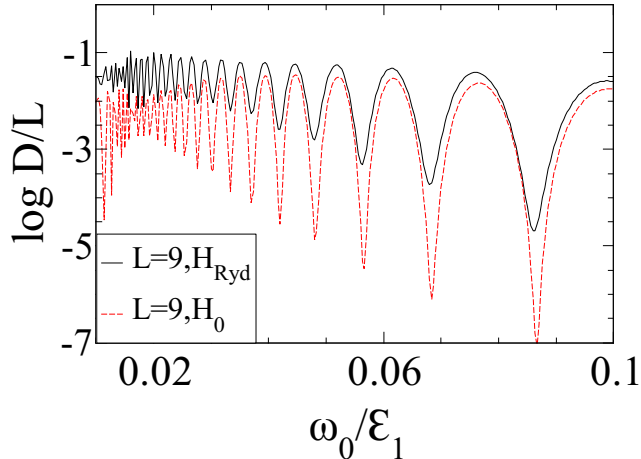


FIG. 9: (Color online) A comparison of periodic dynamics of H_0 (theoretical dipole model) and H_{Ryd} (experimentally emulated Rydberg chain) for $L = 9$. The plot shows $\log[D(T)/L]$ as a function of the drive frequency ω_0/\mathcal{E}_1 . Here L is scaled in units of lattice spacing a .

for experimental detection of Kibble-Zurek behavior and identification of the corresponding critical exponents in such systems.

For the periodic protocol, we focus on drives which take the system twice through the critical points starting from the uniform Mott state. We find a clear signature of dynamic freezing for a range of experimentally relevant drive frequencies. At the freezing frequencies ω_0^* , the system wavefunction, after a drive period, show near unity overlap with the initial ground state leading to near-zero dipole density for our chosen protocol. We also show that this phenomenon leads to an oscillatory behavior in the average oscillation amplitude of the excitation density D^{av} with distinct minima at $\omega_0 = \omega_0^*$ and linear scaling with $\omega_0 - \omega_0^*$ around this point. We note that similar oscillations of excitation density of a Rydberg chain which has similar critical points following a quantum quench have been experimentally observed in Ref. 3. We therefore expect that the measurement of $D^{\text{av}}(t)$ following a periodic drive shall lead to experimental observation of the freezing phenomenon discussed in this work.

Experimental verification of our work could be done using analogous setting of experiments carried out recently in Ref. 3. In this context, we note that the experimental system uses a chain of Rydberg atoms whose Hamiltonian is given by H_{Ryd} (Eq. 4). The equilibrium features of the ground states of H_{Ryd} is shown to be identical to that of the boson Hamiltonian H_0 (Eq. 3); in fact, the density of the Rydberg excitations for H_{Ryd} can be directly mapped to the dipole density of H_0 ³. Both these Hamiltonians support Z_3 and Z_4 symmetry broken ground states separated from the uniform Mott state by quantum criti-

cal points. In fact, the main difference between the two systems comes from the nature of the dipole interaction term; for H_0 , this is implemented through a hard constraint condition (which excludes a certain class of states from the system Hilbert space) while for H_{Ryd} , the interaction term has a finite range and a tunable magnitude. This difference between the two models is not important for their ground state symmetries provided the amplitude of the interaction term can be tuned appropriately; however, there is no reason for the dynamics of the two to be similar. Indeed, it has been noted in Ref. 3, that while both the models exhibit robust short time oscillations following a quench, their long-time dynamical behaviors which has contribution from a significant fraction of states in the Hilbert space is indeed quite different³. Here we would like to note that a comparison between periodic dynamics of H_{Ryd} and H_0 with a chain of length $L = 9$, shown in Fig. 9, seems to indicate that the short time periodic dynamics of both the model exhibits dynamic freezing; the position of the freezing frequencies ω_0^* are identical for both the models whereas the numerical values of $D(T)$ at the freezing frequencies differ. Thus we expect that our theoretical predictions for periodic dynamics could be verified easily using experimental setup of Ref. 3. Also since slow ramp dynamics do not involve participation from all states in the system Hilbert space, we expect the ramp dynamics of both the model to be qualitatively similar leading to possibility of verification of the Kibble-Zurek law; a direct verification of this expectation would involve numerics with longer Rydberg chain which is outside the scope of the current work.

The specific experiments we suggest would use an experimental platform similar to those already implemented in Ref. 3. We envisage a linear ramp of the detuning parameter Ω (Eq. 4) such that a chain of Rydberg atoms at the uniform Rydberg vacuum state reaches the critical point with a rate τ^{-1} at the end of the drive. Our prediction is that the excitation density measured after such a ramp would exhibit Kibble-Zurek scaling for a range of τ^{-1} ; the extent of this scaling regime would increase with L . Moreover, a periodic variation of Ω which takes the system through the critical point to the symmetry broken ground state and back to the Rydberg vacuum state would exhibit dynamic freezing; a measurement of the number of Rydberg excitations after the drive would show near-zero excitation density at specific frequencies.

In conclusion, we have studied the ramp and periodic dynamics of ultracold bosons in the presence of an electric field and repulsive interaction. The model studied supports similar translational symmetry broken ground states and critical points as the Rydberg chain experimentally emulated recently. We have shown that a study of ramp dynamics of the model may lead to verification of the Kibble-Zurek scaling law via measurement of excitation (dipole) density and pointed out the range of drive frequencies where the scaling phenomenon is expected occur. We have also studied the periodic dynamics of the model and shown near-perfect dynamical freezing at

specific frequencies due to a many-body version of Stuckelberg interference which can be tested using Rydberg atom based experimental systems³.

Acknowledgments

The authors thank S. Sachdev and H. Pichler for valuable discussion. R.G. thanks CSIR, India for support

through SPM fellowship. The work of A.S. is partly supported through the Partner Group program between the Indian Association for the Cultivation of Science (Kolkata) and the Max Planck Institute for the Physics of Complex Systems (Dresden). KS thanks Indo-Russian grant (DST INT/RUS/RFBR/P-249 and RFBR grant 16-52-45011, India) for support.

-
- ¹ M. Greiner, O. Mandel, T. Esslinger, T. W. Hansch, I. Bloch, *Nature* (London) **415**, 39 (2002); C. Orzel, A. K. Tuchman, M. L. Fenselau, M. Yasuda, and M. A. Kasevich, *Science* **291**, 2386 (2001).
- ² J. Simon, W. Bakr, R. Ma, M. E. Tai, P. Preiss, and M. Greiner, *Nature* (London) **472**, 307 (2011); W. Bakr, A. Peng, E. Tai, R. Ma, J. Simon, J. Gillen, S. Foelling, L. Pollet, and M. Greiner, *Science* **329**, 547 (2010).
- ³ H. Bernien, S. Schwartz, A. Keesling, H. Levine, A. Omran, H. Pichler, S. Choi, A. S. Zibrov, M. Endres, M. Greiner, V. Vuletic, and M. D. Lukin, arXiv:1707.04344 (unpublished).
- ⁴ I. Bloch, J. Dalibard, and W. Zwerger, *Rev. Mod. Phys.* **80**, 885 (2008).
- ⁵ S. Sachdev, K. Sengupta, and S. M. Girvin, *Phys. Rev. B* **66**, 075128 (2002).
- ⁶ S. Pielawa, T. Kitagawa, E. Berg, and S. Sachdev, *Phys. Rev. B* **83**, 205135 (2011); S. Pielawa, E. Berg, and S. Sachdev, *Phys. Rev. B* **86**, 184435 (2012).
- ⁷ K. Sengupta, S. Powell, and S. Sachdev, *Phys. Rev. A* **69**, 053616 (2004).
- ⁸ C. P. Rubbo, S. R. Manmana, B. M. Peden, M. J. Holland, and A. M. Rey, *Phys. Rev. A* **84**, 033638 (2011)
- ⁹ A. Tomadin, R. Mannella, and S. Wimberger, *Phys. Rev. A* **77**, 013606 (2008); A. R. Kolovsky, *Phys. Rev. A* **70**, 015604 (2004).
- ¹⁰ M. Kolodrubetz, D. Pekker, B. K. Clark, and K. Sengupta, *Phys. Rev. B* **85**, 100505 (2012).
- ¹¹ U. Divakaran and K. Sengupta, *Phys. Rev. B* **90**, 184303 (2014).
- ¹² S. Kar, B. Mukherjee, and K. Sengupta, *Phys. Rev. B* **94**, 075130 (2016).
- ¹³ P. Fendley, K. Sengupta, and S. Sachdev, *Phys. Rev. B* **69**, 075106 (2004).
- ¹⁴ It has been predicted in Ref. 13 that a narrow incommensurate phase would lie between the dipole vacuum and the Z_3 or Z_4 symmetry broken phases. However, such a phase has not been found in numerical studies on finite-sized systems.
- ¹⁵ Finite-size scaling data for both Z_3 and Z_4 critical points appears consistent with $z = 1$ and $\nu = 5/6$ (for Z_3 with $L \leq 21$) and $\nu = 2/3$ (for Z_4 with $L \leq 24$).
- ¹⁶ R. J. Baxter, *J. Phys. C: Solid St. Phys.* **6**, L445 (1973).
- ¹⁷ T. W. B. Kibble, *J. Phys. A* **9**, 1387 (1976); W. H. Zurek, *Nature* (London) **317**, 505 (1985).
- ¹⁸ A. Polkovnikov, K. Sengupta, A. Silva, and M. Vengalattore, *Rev. Mod. Phys.* **83**, 863 (2011); J. Dziarmaga, *Adv. Phys.* **59**, 1063 (2010).
- ¹⁹ F. Y. Wu, *Rev. Mod. Phys.* **54**, 235 (1982).
- ²⁰ A. Das *Phys. Rev. B* **82**, 172402 (2010).
- ²¹ S. Mondal, D. Pekker, and K. Sengupta, *Europhys. Lett.* **100**, 60007 (2012).
- ²² For a review see S. N. Shevchenko, S. Ashhab and F. Nori, *Phys. Rep.* **492**, 1 (2010).
- ²³ C. De Grandi, A. Polkovnikov, and A. W. Sandvik, *Phys. Rev. B* **84**, 224303 (2011).
- ²⁴ The 2D classical 4-state Potts model shows pseudo first-order behaviour near criticality that vanishes in the thermodynamic limit [S. Jin, A. Sen, and A. W. Sandvik, *Phys. Rev. Lett.* **108**, 045702 (2012)]. However, no such signature is found for the sizes studied here in the 1D quantum model with 4-state Potts criticality.